Development (2022) 149, dev200353. doi:10.1242/dev.200353

Fig. 6. Laminin 511 supports NPC identity gene expression. (A-E) RNA-seq analysis of DIV28 CHIR cells after 48 h treatment in different combinations of laminin (laminin 511, msl) and medium (CHIR alone, CHIR; CHIR plus DAPT, DAPT). *n*=3 biological replicates per condition. (A) Transcriptome PCA. (B) The pie-donut diagram shows the proportions of DE genes between the conditions shown in legend (inner pie) and the contribution of up- and downregulation (UP and DOWN in the external donut). The Venn diagram shows the number of genes common to different experimental conditions. Significant differential expression was obtained by NOIseqBIO analysis (q>0.95). (C) GO term enrichment of DE genes between CHIR-511 and CHIR-msl conditions. The most enriched terms are reported, with FDR values ranging from $4.3\times e^{-17}$ to $2.17\times e^{-7}$ for upregulated genes and from $4.7\times e^{-4}$ to $1.5\times e^{-2}$ for downregulated genes. Z-scores were calculated by the GOplot package (R Cran). LogFC: log2(fold change). (D) Diagram reporting the log2(fold change) (log2FC) of selected DE genes between CHIR-511 and CHIR-msl conditions. DE genes were determined by NoiseqBIO (probability, q>0.95). (E) Diagram of focal adhesion gene pathway (KEGG-pathway hsa04510) enriched in the comparison between CHIR-511 and CHIR-msl conditions (FDR: $2.15\times e^{-9}$, *n*=24 genes, 7.14%). PathView package (Bioconductor) was used to generate the red-green heat colour code showing the levels of log2(fold change) gene expression. Coloured genes are differentially expressed between the two conditions.

17.14%). Consequently, the ratio of genes differentially expressed when shifting from laminin 511 to msl is much higher than the ratio when shifting from CHIR to CHIR+DAPT on the same laminin type (Fig. 6B, pie-donut chart). According to the known effect of Notch signalling inhibition by DAPT treatment, the Notch pathway genes *DLK1* and *HES1*, and the NPC marker NES, are differentially expressed between DAPT-treated and untreated cells, in the presence of msl. Moreover, the genes differentially expressed in these cells are significantly enriched in GO terms related to neuronal differentiation. Conversely, the genes differentially expressed between DAPT-treated and control cells, when cultured on laminin 511, are much fewer and show neither differential expression of markers of Notch signalling nor significant GO term enrichment, indicating that cells cultured on laminin 511 are less permissive than cells cultured on msl in responding to DAPT treatment (Fig. 6B, pie-donut chart). Finally, most of the genes upregulated and downregulated during the shift from laminin 511 to msl are shared between DAPT-treated and untreated cells, suggesting that the signalling induced by the laminin type prevails over Notch signalling inhibition (Fig. 6B, Venn diagram).

We focused on the nature of the genes differentially expressed depending on the laminin type (Table S3). The number of genes upregulated in cells cultured on laminin 511 is higher than the number of downregulated genes. This is reflected by the higher degree of GO term enrichment of upregulated genes (Fig. 6C). Genes highly expressed in cells cultured on laminin 511 are mainly enriched in terms related to the focal cell adhesion process whereas genes more expressed in msl-cultured cells belong to terms related to neuronal cell differentiation. To gain a deeper insight, we looked at the expression of selected genes among the most differentially expressed genes, which are known for their role in processes of NPC growth and differentiation. The analysis indicates that laminin 511 in general sustains NPC division, NPC viability and cell signalling, while msl supports chromatin remodelling, neuronal identity transcriptional control and NPC differentiation (Fig. 6D). Accordingly, most of the genes within the top enriched term, i.e. focal adhesion (KEGG_pathway, hsa04510), are downregulated during the shift from laminin 511 to msl (Fig. 6E). These include genes encoding extracellular and intracellular signalling molecules, and cyclin D, and might account for the dramatic effect of laminin 511 in supporting the expansion of the hippocampal neurogenic niche.

NPCs maintained in CHIR and laminin 511 for a long period retain the capacity to generate neurons

We assayed old CHIR cultures for their capacity to differentiate on msl, analysing NEUN and ZBTB20 expression (Fig. S6A, Fig. 7A). We found that, at DIV170, ZBTB20 was significantly upregulated in CHIR-DAPT-treated cells compared with DIV28 CHIR cells, although not to the same extent as in DIV50 CHIR-DAPT treatment, while NEUN was equally upregulated at both culture times. We concluded that older cultures maintain a hippocampal identity and the ability to undergo neuronal differentiation upon Notch inhibition. However, the significant difference in ZBTB20 expression suggested a change of identity between early and late CHIR cells. In fact, DIV50 and DIV170 CHIR cells show many DE genes (Fig. S6B). To delve deeper into this difference, we analysed the expression of a panel of genes specific for dentate gyrus (DG) or CA1-CA3 identity (Cembrowski et al., 2016). We observed that DIV50 CHIR-DAPT cells upregulated both DG and CA1-CA3 markers compared with DIV28 CHIR cells, indicating that these cultures can differentiate into all the different hippocampal mature neuronal cell types (Fig. 7B). Conversely, DIV170 CHIR-DAPT cells upregulated DG markers and downregulated CA1-CA3 markers compared with DIV28 cells (Fig. 7B). We speculate that late cultures behave as mature hippocampus, retaining the ability to produce DG granule cells but incapable of generating new CA1-3 neurons. Notably, this is the expected outcome of adult hippocampal neurogenesis from sub-granular zone (SGZ) progenitors (Gonçalves et al., 2016), although also parallels the expected maturation timing of CA epithelium and dentate epithelium in rodents (Altman and Bayer, 1990). Eventually, we analysed the nature of genes differentially expressed between DIV50 and DIV170 (843 upregulated and 1140 downregulated; Fig. S6B). The analysis of their GO enrichment highlights metabolic and chromatin reorganization processes, including upregulation of transcription factor activity, both RNAPII mediated and non-RNAPII mediated (Fig. S6C), suggesting that these cells might undergo an aging-like process *in vitro*.

Human hippocampal neurons integrate into *in vivo* hippocampus

To compare the capability of early and late CHIR cells to integrate *in vivo*, we labelled DIV30 and DIV180 CHIR cells by mGFP lentiviral transduction and transplanted them into adult mouse dentate gyrus (Fig. 8A,B). Cell survival and integration in the hippocampal circuitry were assessed after ∼3 months. We found neuronal processes of transplanted cells both in the DG around the transplant (Fig. 8B2) and in CA3 (Fig. 8B1). To assess synaptic contacts between grafted and host neurons, GFP^+ fibres in CA3 and DG were labelled with VGLUT1 and PSD-95 (Fig. 9A), and colocalization of GFP, VGLUT1 and PSD-95 was measured (Fig. 9B). We found no differences in terms of % area covered by synapses (Fig. 9C; two-way ANOVA, P=0.158) and synapse density (Fig. 9D; two-way ANOVA, P=0.435) between brain sections containing DIV30 and DIV180 grafted cells.

To compare area and density of DG-CA3 synapses made by grafted cells with those made by host mature hippocampal neurons, we injected Adeno-associated virus (AAV) carrying GFP expression under the synapsin promoter in the DG of adult wild-type mice. Quantification of GFP, VGLUT1 and PSD-95 colocalization showed no differences in terms of area covered by GFP^+ synapses between grafted and AAV infected mice (Fig. 9E; two-way ANOVA, P=0.408). However, we found significant statistical differences in terms of synapses density

Development (2022) 149, dev200353. doi:10.1242/dev.200353

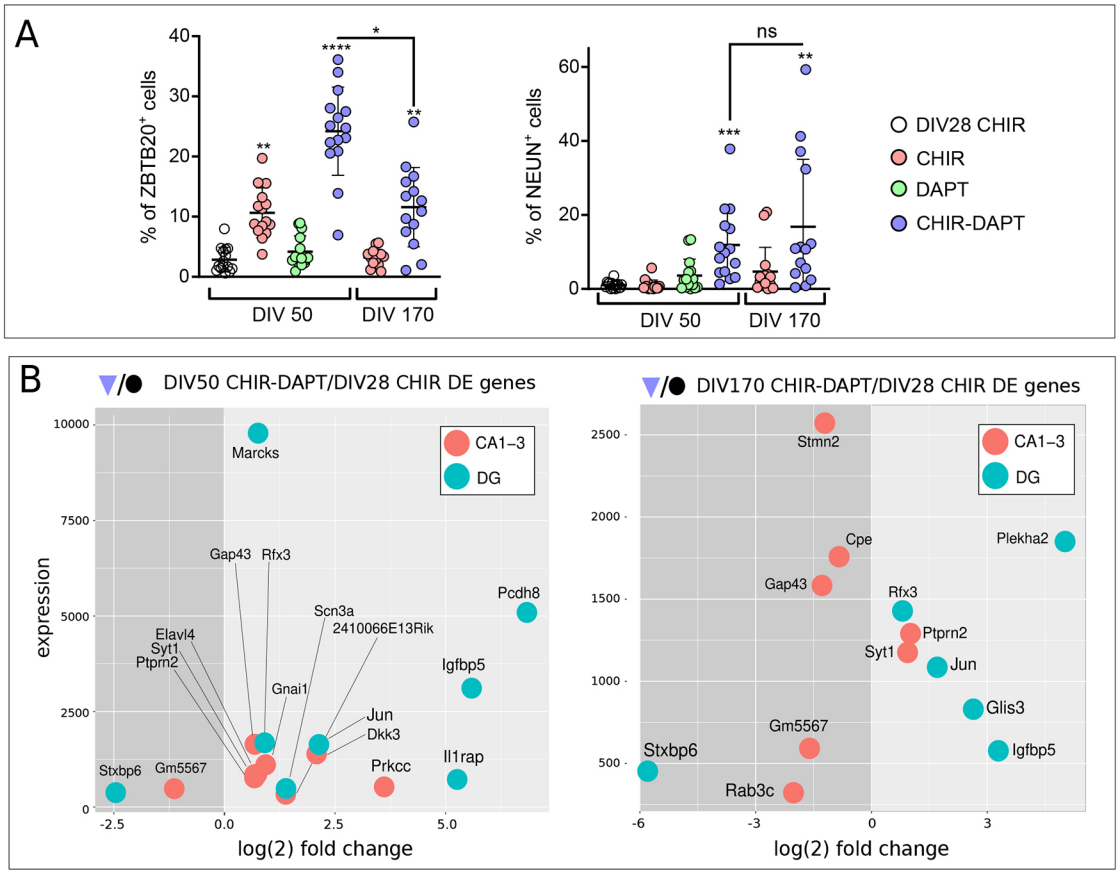

Fig. 7. Early and late CHIR cells maintain neurogenic capacity. (A,B) DIV40 and DIV160 CHIR cells were plated on msl and cultured until DIV50 and DIV170, respectively, in minimal media (Control), or treated at DIV46 and DIV166 for 2 days with CHIR, DAPT or CHIR-DAPT. Inhibitors were removed after 2 days, and cells were maintained in minimal media for 2 more days before analysis (DIV50 and DIV170); *n*=3 biological replicates for each condition. (A) Percentage of cells positive for ZBTB20 and NeuN at the different times and culture conditions, as indicated by labels. Statistical analyses were performed by one-way ANOVA, post-hoc Kruskal–Wallis test; asterisks above plotted values indicate comparison against control, whereas asterisks above solid black bars indicate comparison between groups; error bar represent 99% confidence interval. **P*<0.05, ***P*<0.01, ****P*<0.001, *****P*<0.0001. (B) M-D plots of RNA-seq analysis of markers of DG or CA1-3 layers in cells as in A, differentially expressed between the culture conditions indicated in labels (NOIseq analysis, q>0.8).

between endogenous and grafted fibres (Fig. 9F; two-way ANOVA, P=0.011). In particular, post-hoc comparisons revealed significant differences in the CA3 region (Tukey's test, P=0.033) and a tendency towards a difference in the DG region (Tukey test's, P=0.073). Species-intrinsic differences and time of maturation might have accounted for these observations (see Discussion). Nonetheless, our results confirm that the differentiation and maturation capabilities are retained by hiPSC-derived hippocampal progenitors maintained in the CHIR-laminin 511 niche. Moreover, the area covered by synapses was similar in GFP$^+$ fibres belonging to grafted and endogenous DG neurons, despite the density being higher in host cells.

DISCUSSION

WNT signalling induces a hippocampal cell identity in a narrow time window of hiPSC neuralization

The hippocampus is a fundamental brain structure hosting one of the two adult brain neurogenic niches. Although extensively studied, both extrinsic and intrinsic cues orchestrating cell identity specification, neurogenic activity, layer specification and aging are substantially unsettled in humans. Herein, we established a protocol to simulate hippocampal fating and extended propagation of hippocampus-like neural stem cell populations. WNT signalling is a necessary pathway in hippocampal fating (Grove and Tole, 1999) but also in regulating adult neurogenesis (Arredondo et al., 2020; Ni et al., 2021). CHIR99021 (CHIR), which induces WNT signalling via indirect activation of the β-catenin pathway (Naujok et al., 2014), has previously been used in *in vitro* hippocampal models of hESC and mESC differentiation (Sakaguchi et al., 2015; Terrigno et al., 2018). Here, we demonstrate that CHIR upregulates hippocampal developmental markers to differentiate hiPSCs with an identity similar to hippocampal neuroepithelial cells. Starting from hiPSCs committed to dorsal telencephalic identity (Martins et al., 2021; Shi et al., 2012b), the addition of CHIR to minimal culture medium for 12 days in a specific time window of differentiation is sufficient to generate NPC populations with hippocampal identity. These populations significantly upregulated PROX1, DCX, BCL11B and ZBTB20, which are key markers of embryonic hippocampal cells (Iwano et al., 2012; Knoth et al., 2010; Nielsen et al., 2014; Simon et al., 2012). Moreover, the global gene expression profile of these cells is similar to the profile of human hippocampal embryonic cells, as demonstrated by transcriptome-wide clustering analysis.

The analysis of hippocampal scRNA-Seq datasets confirms that ZBTB20 is one of the most robust markers of hippocampal identity. Using ZBTB20 as reporter, we could assay the different effects of

Development (2022) 149, dev200353. doi:10.1242/dev.200353

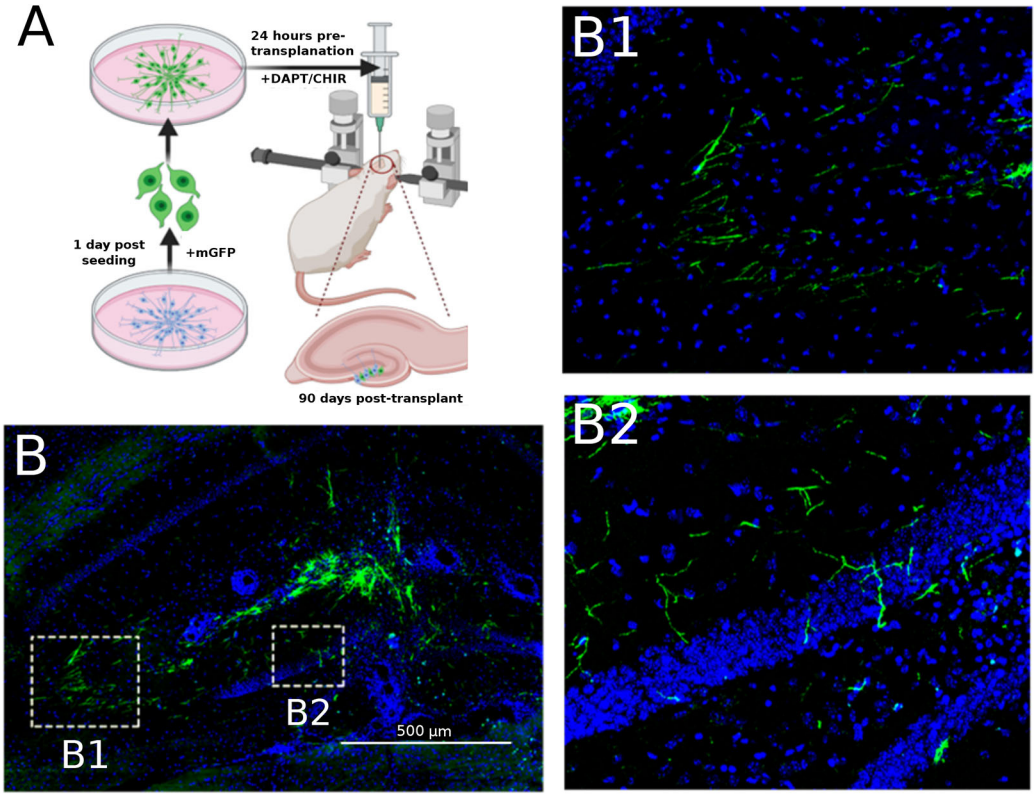

Fig. 8. *In vivo* transplantation of CHIR cells into mouse hippocampal DG. (A) Experimental scheme: after 30 or 180 days *in vitro*, CHIR cells were infected with a GFP-expressing lentiviral vector, treated 24 h with DAPT and transplanted in the DG of adult wild-type mice. (B) Micrograph of the hippocampal grafted cells (GFP+) in the host dentate gyrus (Hoechst). Magnifications of the outlined areas show GFP$^+$ fibres elongated in the peritransplant DG area (B2) and in CA3 (B1).

Notch and WNT signalling in establishing a hippocampal identity in neuralized hiPSCs and found that WNT is necessary for hippocampal specification independently of the state of Notch signalling. This conclusion is further supported by the analysis of GO term enrichment of the genes differentially expressed upon WNT and Notch activation.

Laminin 511 is an essential signalling component of the hippocampal neurogenetic niche

Because the hippocampal niche sustains continuous neurogenesis throughout embryonic and post-natal life, we sought to recreate a model of SGC niche *in vitro*, to further understand the signalling machinery involved. We focused on the ECM component of the niche because it is the least described. Laminins are one of the major protein groups in the extracellular matrix (ECM). They are heterotrimers of five α-, three β- and three γ-subunits with different expression patterns in distinct developing and adult brain regions, and they interact with integrins and non-integrin receptors, such as dystroglycan, mediating cell adhesion and intracellular signalling (Nirwane and Yao, 2019). The mechanisms of laminin signalling have not been completely elucidated. In hiPSCs, laminin 511 binds to α3β1-, α6β1- and α6β4-integrin, inducing activation of the PI3K/AKT-dependent and Ras/MAPK-dependent signalling pathways. Moreover, the interactions of laminin-511 and α6β1-integrin with E-cadherin inhibit apoptosis mediated by the Rho kinase (ROCK) signalling pathway (Nakashima and Omasa, 2016). Most of the studies on the role of laminins and integrins on neural progenitor proliferation and differentiation have been performed in culture or non-mammal models. Laminin stimulates expansion and differentiation of hESC-derived neural progenitors via interaction with α6- or β1-integrin subunits (Ma et al., 2008). Loss of β1-integrin generates smaller neurospheres through MAPK signalling (Campos et al., 2004). Interestingly, overexpression of constitutively active β1-integrin in the embryonic chick mesencephalon enhances the number of mitotic progenitors, analogous to sub-apical progenitors in mouse, through a non-cell autonomous mechanism that is mediated by the upregulation of Wnt7a (Long et al., 2016).

Previous *in vivo* reports have indicated the necessity of α5 laminin subunit in the cortical SVZ niche to propagate neural stem cell populations (Nascimento et al., 2018). We thus compared laminin α5β1γ1 (laminin 511) against other laminin isoforms associated with either neuronal cell survival, such as α1β2γ1 (laminin 121) (Sasaki et al., 2010), laminin isoforms of peripheral epithelial and endothelial niches (α3-β3-β2 and α4-β1-β1; laminin 332 and 411) (Hall et al., 2022; Kiritsi et al., 2013) or a purified mouse laminin isoform (α1-β1-β1; msl) (Horejs et al., 2014). Indeed, we confirmed that laminin 511 exclusively promoted NPC survival and maintenance in comparison with the other four substrates. We then cultured hippocampal NPC populations from DIV 28 onwards, using laminin 511 as the substrate, and found that these populations could be expanded over 200 days *in vitro* with little to no deviation from a progenitor-like condition, as indicated by DCX downregulation. These cells were still able to differentiate if transferred from laminin 511 to msl. The observation that laminin 511 supports continuous expansion of the hippocampal niche sheds light on a new aspect of the hippocampal neurogenic molecular machinery to be addressed in detail in future studies. Here, we report

Development (2022) 149, dev200353. doi:10.1242/dev.200353

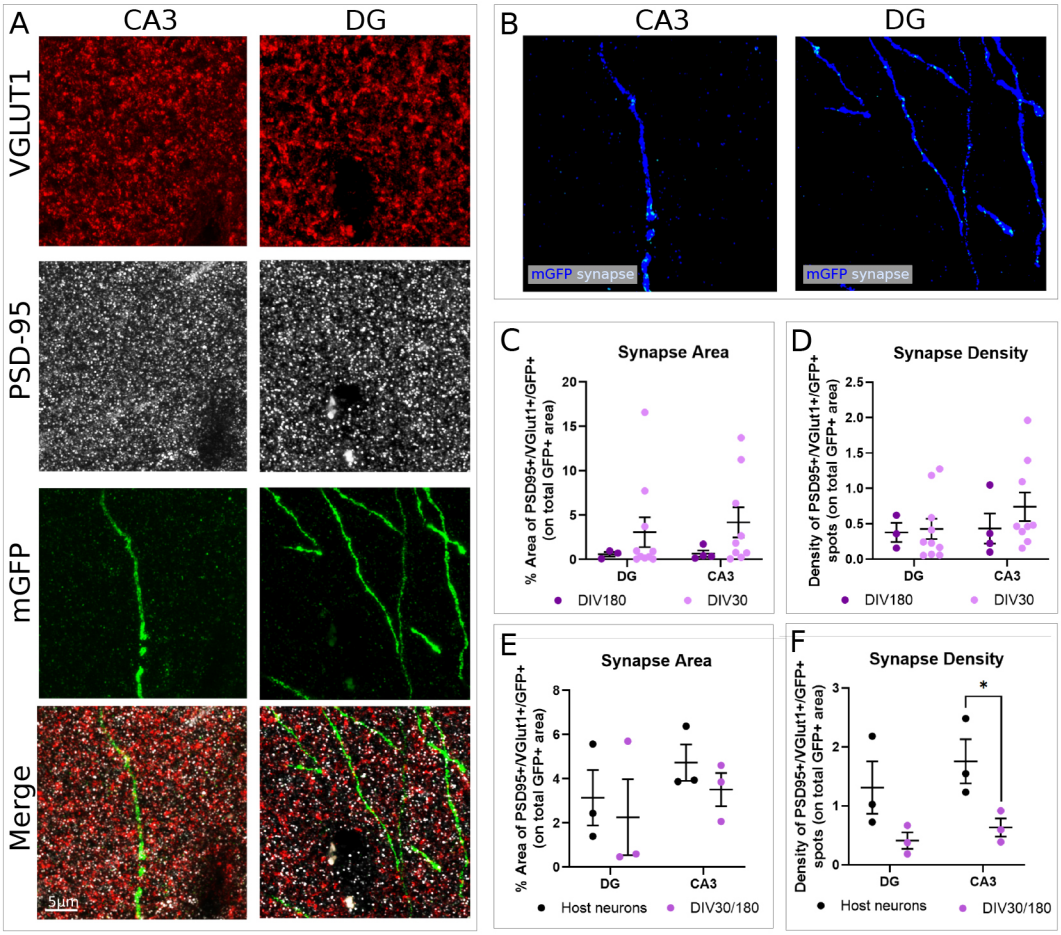

Fig. 9. Quantification of GFP$^+$ synapses in DIV30, DIV180 and host neurons. (A) Immunostaining of VGLUT1, mGFP and PSD-95 in fibres of transplanted and host neurons of CA3 and DG. (B) Synapses of transplanted neurons were imaged considering pixels positive for VGLUT1, PSD-95 and mGFP (light-blue signal). Positive pixels were then superimposed to mGFP (dark-blue signal). (C,D) Synapse quantification was performed considering positive pixels as in B. Synapses were measured in terms of density and percentage of GFP$^+$ area covered by synapses. Comparisons between sections acquired from brains injected with DIV30 and DIV180 CHIR cells showed no statistical differences in terms of percentage of area covered by synapses (two-way ANOVA, P=0.158) (C) and synapses density (two-way ANOVA, P=0.435) (D). DG: n=3 sections (DIV180), n=10 sections (DIV30). CA3: n=4 sections (DIV180), n=9 sections (DIV30). (E) Additionally, the percentage of area covered by synapses was similar between grafted and endogenous hippocampal neurons, which were labelled with a GFP-expressing AAV injected in the DG of wild-type control animals (two-way ANOVA, P=0.408). (F) Nonetheless, synapse density of grafted neurons resulted lower than endogenous neurons in CA3 region (two-way ANOVA, P=0.033) but not in the DG region (two-way ANOVA, P=0.077) (n=3 mice per group). Data are mean±s.e.m.

a preliminary analysis of the mechanisms by which laminin 511 supports the expansion of NPCs in culture. Our analysis of the short-term effects after cell re-seeding on laminin 511 or msl indicates that laminin 511 mostly acts as a key signalling factor influencing gene expression. The results of RNA-seq indicate a dramatic effect of laminin 511 directly or indirectly sustaining the expression of genes related to NPC identity, expansion and viability through the activation of key members of the focal adhesion pathway. We speculate that msl promotes NPC differentiation because of its much lower efficiency than laminin 511 in supporting NPC stemness and proliferation by focal adhesion gene activation. Notably, the extent of gene expression control by laminin 511 is dramatically higher than the control level exerted by Notch signalling. Moreover, the intracellular signalling activated by laminin 511 is sufficient to bypass the Notch signalling, as suggested by the inability of cells cultured on laminin 511 to activate neuronal markers upon DAPT treatment. Our observations suggest a crucial role for laminin components in the hippocampal neurogenic niche and open new routes to the comprehension of the contribution of ECM to hippocampal cell stemness. These include detailed studies of laminin receptor expression in hippocampal progenitors, and their functional role in laminin-directed intracellular signalling.

WNT-laminin 511 niche sustains hippocampal NPC expansion and maturation *in vitro*

The differences of expression of markers of DG and CA1-CA3 layer identity observed between early and late cultures induced to differentiate by msl and DAPT suggest that long-term expansion of hippocampal progenitors within the WNT-laminin 511 niche induced changes in NPC competence. We speculate that our culture conditions somehow prompted NPCs to mature *in vitro* in a way that recapitulates prenatal *in vivo* development: in fact, late cultures keep expressing granule DG markers but downregulate CA1-CA3 markers, as it occurs at the end of pre-natal neurogenesis (Altman and Bayer, 1990; Gonçalves et al., 2016).

The hippocampus is a highly selective brain region with respect to cell survivability and integration, as previous heterologous cell-region transplantations have demonstrated (Quattrocolo et al., 2017;

Development (2022) 149, dev200353. doi:10.1242/dev.200353

Terrigno et al., 2018). Although successful xenografting of hiPSC-derived NPCs into the DG of adult host mice cannot rule out the possibility that the transplanted cells are not bona fide human hippocampal neurons, it indicates that their long-term expansion *in vitro* has not altered their capacity to terminally differentiate and integrate into a host hippocampal tissue. Notably, the analysis of the molecular synaptic markers in the xenografts supports the idea that transplanted and resident neurons generate synapses at a similar extent, because the area of GFP^+ synapses is not significantly different between grafted and AAV-infected mice. However, the synaptic density of the grafted cells is lower than the synaptic density of resident cells. We speculate that this result might be due to intrinsic structural differences of the synapses in and/or between the two species, and we suggest that human-human and human-mouse cell synapses within xenografts might occupy a larger volume compared with mouse-mouse cells synapses.

Finally, our results contribute to understanding the key changes of gene expression occurring during human hippocampus development and indicate a previously unreported role for laminin 511 in supporting the *in vitro* expansion of a hippocampal neurogenic niche. The implications of this study may open new avenues for studying cell type-dependent neurogenesis, synaptic transmission in the hippocampus and future cell-based therapies.

MATERIALS AND METHODS

hiPSC culture and differentiation

For both cell expansion and differentiation, hiPSCs (ATCC, catalogue DYS0100) were seeded onto Geltrex LDEV-Free Reduced Growth Factor Basement Membrane Matrix (Thermo Fisher Scientific, A1413202) in Essential 8 Medium (Thermo Fisher Scientific, A1517001) containing Essential 8 Medium Supplement (Thermo Fisher Scientific, A1517-01), 100 U/ml penicillin-streptomycin and 2 µM Y-27632 (Cell Guidance Systems, SM02-5). 24 h later, E8 containing Y-27632 was aspirated and fresh E8 medium without Y-27632 was added. E8 medium was changed daily for another 2 days. For neural differentiation, cells were incubated in WNT/BMP/TGF-β triple inhibition (WiBiTi) medium [DMEM/F-12 (Thermo Fisher Scientific, 11320033) containing 2 mM glutamine, 1 mM sodium pyruvate, 100 U/ml penicillin-streptomycin, 1 mM non-essential amino acids, 0.05 mM β-mercaptoethanol, 10 µM 53AH (WNT inhibitor, Cellagen Technology, C5324-2 s), 10 µM LDN193189 hydrochloride (BMP inhibitor, Sigma-Aldrich, SML0559), 1 µM RepSox (Sigma-Aldrich, R0158-5MG, TGFβ inhibitor), N-2 Supplement 100× (Thermo Fisher Scientific, 17502001) and B-27 Supplement minus Vitamin A 50× (Thermo Fisher Scientific, 12587010)]. The day of shift from Essential 8 Medium to WiBiTi medium is DIV 0. WiBiTi medium was changed daily until DIV 10 where cells were passaged and reseeded in N2B27 medium containing Y-27632 at a density of 200,000 cells/cm^2 on culture dish pre-coated with Poly-ornithine (P3655 Sigma-Aldrich; 20 µg/ml in sterile water, 24 h coating at 37°C) and laminin iMatrix-511silk E8 (human laminin 511, Amsbio, AMS.892 021, 24 h coating at 37°C). Less than 24 h later, N2B27 containing Y-27632 was aspirated and fresh WiBiTi medium without Y-27632 was added. Cells were maintained in WiBiTi medium for another 4 days until DIV 15, where the medium was changed to N2B27.

To induce hippocampal identity, the following day (DIV 16) cells were then cultured for an additional 6 days (DIV 21) in CH27 medium (N2B27 medium supplemented with 3 µM CHIR99021; Sigma-Aldrich, SML1046-5MG). At DIV 21, cells reached confluence and required another passage in CH27 medium supplemented with Y-27632 and onto poly-ornithine/laminin 511-coated plastic at a density of 200,000 cells/cm^2. Less than 24 h later, CH27 containing Y-27632 was aspirated and fresh CH27 medium without Y-27632 was added. Medium was changed daily with fresh CH27 until DIV 28 wherein cells, named CHIR cells, were passaged for longitudinally maintaining the CHIR NSC niche or used for differentiation experiments.

When different laminins were used, Poly-ornithine was pre-coated for 24 h at 37°C, followed by coating with 2.5 µg/ml of specific laminin in PBS for 24 h at 37°C. The following laminins were used: natural mouse laminin (msl, 111, 23017015, Thermo Fisher Scientific); laminin 121, Biolaminin 121 LN (LN121); laminin 332, Biolaminin 332 LN (LN332); and laminin 441, Biolaminin 441 LN (LN441).

Maintaining hippocampal NSC niche

Starting from DIV 28, CHIR NPCs were passaged and reseeded in N2B27 medium containing Y-27632 at a density of 100,000 cells/cm^2 on poly-ornithine/511 human laminin-coated plastic. Less than 24 h later, CH27 containing Y-27632 was aspirated and fresh CH27 medium without Y-27632 was added. CH27 medium was changed daily for 2 weeks from the reseeding date (DIV 42) whereupon cells were passaged again in an identical manner until DIV 200. Approximate cell counts were recorded per split and sample pellets for qRT-PCR were also collected.

hiPSC-derived NPC differentiation

NPCs, regardless of age, do not differentiate on laminin 511 and attempted differentiation resulted in cell detachment and death. When ready to differentiate, either endogenously or by Notch inhibitor (DAPT), CHIR cells were seeded onto plates coated with poly-ornithine msl. For immunocytodetection, cells were seeded onto Eppendorf biofilm-bottom plates (Eppenforf, EP0030722019) or on a layer of mESC-derived hippocampus neurons, derived using the protocol of Terrigno et al. (2018). After passaging/thawing, cell suspensions were centrifuged at 200 ***g*** for 4 min and the cell pellet resuspended in CH27 supplemented with Y-27632. Less than 24 h later, CH27 containing Y-27632 was aspirated and fresh CH27 medium without Y-27632 was added. Medium was changed daily with fresh CH27 until cells reached 90% confluence (after ∼10 days), whereupon CH27 medium was changed to medium containing DMEM/F-12, 2 mM glutamine, 1 mM sodium pyruvate, 100 U/ml penicillin-streptomycin, 0.05 mM β-mercaptoethanol, N-2 supplement (100×), B-27 supplement (50×) (with Vitamin A, Thermo Fisher Scientific, 125870-01), 20 ng/ml recombinant human BDNF (NBP2-52006, Novus Biologicals) and 0.5 mM ascorbate (A92902, Sigma-Aldrich). Experimental differentiation medium included 3 µM CHIR99021 (CHIR) or 12.5 µM DAPT (Sigma-Aldrich D5942), or both.

Cell culture imaging

Cells were fixed for 10 min in 2% paraformaldehyde, permeabilized and blocked in 3% foetal calf serum, 3% bovine serum albumin and 0.2% Triton in PBS at room temperature for 1 h. Primary antibodies were incubated at 4°C in PBS, 3% FCS and 3% BSA ranging from overnight (for cytoskeletal/membrane proteins) up to 72 h (for nuclear antigens). Secondary antibody was incubated under the same conditions for ∼1.5 h at room temperature. After PBS washes and nuclear staining with Hoechst, cells were mounted in Aqua/Poly-mount (Polysciences, 18606-100) and stored at 4°C before imaging. Images were produced on a Leica SP2 confocal microscope or Zeiss confocal microscope by acquiring *z*-stack images 10-15 optical slices thick, each slice ∼1 µm.

Previously released ImageJ macros (https://imagej.net/scripting/batch) were employed to batch analyse stack fluorescence parameters, including fluorescent signal magnitude and density, fluorescent cell count, total approximate fibre length, conversion of full experiment stacks to individual component TIFFs and conversion of full experiment stacks to the compressed single channel representative PNGs. The only parameters changed were cell area, which is dependent on the objective, and binary threshold, which is dependent on the relative signal-to-noise ratio of fluorescence marker in an independent experiment.

RNA extraction

All *in vitro* samples used for transcriptomic assays were harvested by 5′, 37°C trypsinization. Detached cells were homogeneously suspended in solution, collected in microcentrifuge tubes and pelleted at 200 ***g*** for 5 min. After centrifugation, the supernatant was aspirated and the cell pellet was disrupted and processed using NucleoSpin RNA kit (Machery-Nagel, 740955.250). RNA concentration was measured using a NanoDrop Lite Spectrophotometer (Thermo Fisher Scientific, ND-LITE).

Development (2022) 149, dev200353. doi:10.1242/dev.200353

qRT-PCR analysis of human and mouse cells

RNA extracted from *in vitro* samples were processed using Reverse Transcriptase Core Kit 300 (Eurogentec, RT-RTCK-03). Approximately 200 ng of RNA was reverse transcribed into cDNA for qRT-PCR analysis. SensiFAST SYBR mix (12 µl, BioLine, BIO-98020) and cDNA (8 µl) were combined in 4titude PCR quality tubes and quantified using Qiagen 72-Well Rotorgene as previously described (Terrigno et al., 2018).

RNA-seq

RNA-seq libraries were prepared with either the SMART-Seq HT PLUS Kit (Takara; used for CHIR differentiation experiments) or the Stranded Total RNA Prep with Ribo-Zero Plus Kit (Illumina; used for laminin comparison) following manufacturer's instructions. Pooled reads were sequenced on a NovaSeq machine (Illumina), obtaining between 20 and 50 M reads per sample.

Transcripts were pseudoaligned using Salmon (Patro et al., 2017) in mapping-based mode (with its default '–validateMappings' flag). A decoy-aware version of the Ensembl mouse transcriptome (mm10; http://refgenomes.databio.org/) was used as a reference. RNA-seq analysis was carried out using the R package NOISeq. Raw counts were normalized with the Trimmed Mean of M values (TMM) method. Low-count filtering was performed with the CPM method, using cpm=1 as threshold. PCA exploration was carried out to confirm that the experimental samples were clustered according to the experimental design (see Fig. 2A, Fig. 6A). Differential expression was calculated by the NOISeq or NOISeqBIO method and a significance threshold of q=0.8 or q=0.95 was applied, respectively. RNA-seq data from Allen Brain Atlas (Colantuoni et al., 2011) were compared with hiPSCs data upon scaling of both datasets to percent and by applying the hclust (distance) and prcomp R Cranpackages. Raw genomic data and expression counts have been deposited in the Gene Expression Omnibus database under accession number GSE199355.

COTAN analysis of scRNA seq dataset

Co-expression table analysis (COTAN) (Galfrè et al., 2021) was used to find an approximation of the probability of zero read counts for a gene in a cell, testing the null hypothesis of independent expression for gene pairs, by counting zero/non-zero unique molecular identifier (UMI) counts in single cells. Expected values for contingency table analysis were obtained using UMI detection efficiency (UDE), average expression of genes was estimated using linear method and gene dispersion was estimated by fitting the observed number of cells with zero UMI count. COTAN provided both an approximate *P*-value for the test of independence and a signed co-expression index (COEX), which measures the direction and intensity of the deviation from the independence hypothesis. Plots were generated with ggplot2 in R environment. The following R Cran packages were employed: matrixStats, ggfortify, dplyr, rray, propagate, data.table, ggsci, gmodels, parallel, tibble and ggrepel.

In vivo assay of neural precursors survival and integration

All experiments were carried out in accordance with the EU Council Directive 2010/63/EU on the protection of animals used for scientific purposes, and were approved by the Italian Ministry of Health (authorization number 739/2017-PR). Mice were housed in standard conditions with water and food *ad libitum* and a 12 h dark/light cycle. A total of 13 C57BL6/J mice were used, five were grafted with DIV30 cells, five with DIV180 cells and three mice were injected with AAV-GFP as controls. Mice injected with cells were treated daily with subcutaneous injections of cyclosporine A (Sandimmun, 10 mg/kg) from the day before the injection to 3 weeks after and then cyclosporine A was delivered in the drinking water (Sporimune, 0.21 mg/ml) and refreshed every 3 days. Of the 10 cell-injected mice, one DIV30 died post-surgery, two DIV30 and two DIV180 showed no successful grafts in the DG, three DIV180 showed a small graft with few fibres (not reaching the CA3). One DIV180 and two DIV30 mice showed a considerable amount of fibres in both CA3 and DG; thus, only these animals were considered in the synapse quantification.

On the day of the transplantation, cells were detached from culture substrate by removing culture medium, washing with 1× Versene (Thermo Fisher Scientific, A4239101) and incubating with minimal volume of Accutase (A6964, Sigma-Aldrich) for 25 min at 37°C. At the end of the incubation, Accutase was diluted in fresh 1× PBS in a volumetric ratio of 1 Accutase:10 PBS. Cell suspension was centrifuged at 1700 ***g*** for 4 min at room temperature and resuspended in a volume of foetal bovine serum sufficient to concentrate cells at 100,000 cells/µl. Cells were maintained at 4°C until they were injected. Mice were anesthetized using a cocktail of hypnorm (0.38 mg/kg) and hypnovel (12 mg/kg), and placed in a stereotaxic frame. The scalp was opened and the head bone sutures exposed for reference. Cells (100,000 cells/µl) were injected in the dentate gyrus through three injection sites (2, 1.7 and 2.3 mm A; 1.5 mm ML; 1.7 mm DV from Bregma), delivering 0.5 µl for each site, using a Hamilton syringe connected to a motorized pump (Legato130). Cells were gently resuspended, loaded (2 µl, 2 µl/min) in the syringe and infused (0.3 µl/min) in the three brain sites. After the injection, the syringe was left in place for 2 min, before being removed, emptied and washed with saline and cell medium. The skin was sutured and mice were placed on a heating pad and allowed to waken.

Imaging of human cells in mouse hippocampal sections

At 3 months post-transplantation, mice were transcardially perfused with PFA 4%. Brains were collected and sliced using a freezing microtome, to obtain 30 µm coronal sections. After 1 h in blocking solution, free-floating sections were incubated overnight with primary antibodies anti-GFP (goat, Abcam), anti-PSD95 (rabbit, Abcam) and anti-VGLUT1 (guinea pig, SYSY). After rinsing, secondary antibodies (Alexa488 anti-goat, CY5 anti-rabbit and RRX anti-guinea pig, Jackson) were used for immunostaining. Cell nuclei were stained using Hoechst. For antibody details, see Table S4.

Images for synapse quantification were acquired with a Plan Apochromat 63×/1.4 NA oil DIC M27 objective lens with a Axio Observer 7 microscope on a LSM 900 Airyscan2 confocal (Carl Zeiss) equipped with 488, 561 and 640 lasers. The total thickness of the *z* stacks was 2-3 µm and the distance between adjacent focal planes was set at a constant value of 0.15 µm intervals.

For each animal (n=6), one field in CA3 and one in the DG region were acquired in at least three sections with visible GFP+ fibres. Stacks were opened in ImageJ2/Fiji (https://imagej.net/software/fiji/), using a custom-made macro, each channel was thresholded and only particles with an over threshold signal in all three channels were considered and counted as synapses. Using a Matlab custom-made script, for each plane, total area and number of selected synapses were expressed as percentage of total GFP^+ threshold area, and then averaged among focal planes of each stack.

Acknowledgements

We thank M. A. Calvello and V. Liverani for technical support; L. Conti for induced pluripotent stem cell neural differentiation methods advice; and Dr D. Vozzi and the IIT Neurogenomics facility for transcriptomic library sequencing. We are immensely grateful to M.C. for his contribution as a scientist and man.

Competing interests

The authors declare no competing or financial interests.

Author contributions

Conceptualization: M.C., L.P., C.A., F.C.; Methodology: K.D., F.T., E.N., A.C., V.M., F.B., L.P., C.A.; Software: S. Galfrè; Formal analysis: K.D., S. Gustincich, M.C., L.P., C.A.; Investigation: K.D., E.N., A.C., V.M., A.M.F.; Resources: S. Gustincich, M.C., L.P., C.A.; Data curation: K.D.; Writing - original draft: K.D., L.P.; Writing - review & editing: C.A., L.P., F.C.; Supervision: F.C.; Project administration: F.C.

Funding

This work was supported by the European Commission FP7 PAIN-CAGE project (603191) and by the H2020 LEIT Information and Communication Technologies 2016 MADIA project (732678).

Data availability

Raw genomic data and expression counts have been deposited in GEO under accession number GSE199355.

References

Abellán, A., Desfilis, E. and Medina, L. (2014). Combinatorial expression of Lef1, Lhx2, Lhx5, Lhx9, Lmo3, Lmo4, and Prox1 helps to identify comparable subdivisions in the developing hippocampal formation of mouse and chicken. *Front. Neuroanat.* **8**, 59. doi:10.3389/fnana.2014.00059

Åberg, M. A. I., Åberg, N. D., Hedbäcker, H., Oscarsson, J. and Eriksson, P. S. (2000). Peripheral infusion of IGF-I selectively induces neurogenesis in the adult rat hippocampus. *J. Neurosci.* **20**, 2896-2903. doi:10.1523/JNEUROSCI.20-08-02896.2000

Ables, J. L., Decarolis, N. A., Johnson, M. A., Rivera, P. D., Gao, Z., Cooper, D. C., Radtke, F., Hsieh, J. and Eisch, A. J. (2010). Notch1 is required for maintenance of the reservoir of adult hippocampal stem cells. *J. Neurosci.* **30**, 10484-10492. doi:10.1523/JNEUROSCI.4721-09.2010

Altman, J. and Bayer, S. A. (1990). Migration and distribution of two populations of hippocampal granule cell precursors during the perinatal and postnatal periods. *J. Comp. Neurol.* **301**, 365-381. doi:10.1002/cne.903010304

Altman, J. and Das, G. D. (1965). Autoradiographic and histological evidence of postnatal hippocampal neurogenesis in rats. *J. Comp. Neurol.* **124**, 319-335. doi:10.1002/cne.901240303

Arredondo, S. B., Guerrero, F. G., Herrera-Soto, A., Jensen-Flores, J., Bustamante, D. B., Oñate-Ponce, A., Henny, P., Varas-Godoy, M., Inestrosa, N. C. and Varela-Nallar, L. (2020). Wnt5a promotes differentiation and development of adult-born neurons in the hippocampus by noncanonical Wnt signaling. *Stem Cells* **38**, 422-436. doi:10.1002/stem.3121

Asrican, B., Wooten, J., Li, Y.-D., Quintanilla, L., Zhang, F., Wander, C., Bao, H., Yeh, C.-Y., Luo, Y.-J., Olsen, R. et al. (2020). Neuropeptides modulate local astrocytes to regulate adult hippocampal neural stem cells. *Neuron* **108**, 349-366.e6. doi:10.1016/j.neuron.2020.07.039

Berdugo-Vega, G., Arias-Gil, G., López-Fernández, A., Artegiani, B., Wasielewska, J. M., Lee, C.-C., Lippert, M. T., Kempermann, G., Takagaki, K. and Calegari, F. (2020). Increasing neurogenesis refines hippocampal activity rejuvenating navigational learning strategies and contextual memory throughout life. *Nat. Commun.* **11**, 135. doi:10.1038/s41467-019-14026-z

Bettio, L. E. B., Rajendran, L. and Gil-Mohapel, J. (2017). The effects of aging in the hippocampus and cognitive decline. *Neurosci. Biobehav. Rev.* **79**, 66-86. doi:10.1016/j.neubiorev.2017.04.030

Brandhorst, S., Choi, I. Y., Wei, M., Cheng, C. W., Sedrakyan, S., Navarrete, G., Dubeau, L., Yap, L. P., Park, R., Vinciguerra, M. et al. (2015). A periodic diet that mimics fasting promotes multi-system regeneration, enhanced cognitive performance, and healthspan. *Cell Metab.* **22**, 86-99. doi:10.1016/j.cmet.2015.05.012

Campos, L. S., Leone, D. P., Relvas, J. B., Brakebusch, C., Fässler, R., Suter, U. and Ffrench-Constant, C. (2004). β1 integrins activate a MAPK signalling pathway in neural stem cells that contributes to their maintenance. *Development* **131**, 3433-3444. doi:10.1242/dev.01199

Cembrowski, M. S., Wang, L., Sugino, K., Shields, B. C. and Spruston, N. (2016). Hipposeq: a comprehensive RNA-seq database of gene expression in hippocampal principal neurons. *Elife* **5**, e14997. doi:10.7554/eLife.14997

Charvet, C. J. and Finlay, B. L. (2018). Comparing adult hippocampal neurogenesis across species: translating time to predict the tempo in humans. *Front. Neurosci.* **12**, 706. doi:10.3389/fnins.2018.00706

Colantuoni, C., Lipska, B. K., Ye, T., Hyde, T. M., Tao, R., Leek, J. T., Colantuoni, E. A., Elkahloun, A. G., Herman, M. M., Weinberger, D. R. et al. (2011). Temporal dynamics and genetic control of transcription in the human prefrontal cortex. *Nature* **478**, 519-523. doi:10.1038/nature10524

Galfrè, S. G., Morandin, F., Pietrosanto, M., Cremisi, F. and Helmer-Citterich, M. (2021). COTAN: scRNA-seq data analysis based on gene co-expression. *NAR Genom. Bioinform.* **3**, lqab072. doi:10.1093/nargab/lqab072

Gonçalves, J. T., Schafer, S. T. and Gage, F. H. (2016). Adult neurogenesis in the hippocampus: from stem cells to behavior. *Cell* **167**, 897-914. doi:10.1016/j.cell.2016.10.021

Grove, E. A. and Tole, S. (1999). Patterning events and specification signals in the developing hippocampus. *Cereb. Cortex* **9**, 551-561. doi:10.1093/cercor/9.6.551

Grove, E. A., Tole, S., Limon, J., Yip, L. and Ragsdale, C. W. (1998). The hem of the embryonic cerebral cortex is defined by the expression of multiple Wnt genes and is compromised in Gli3-deficient mice. *Development* **125**, 2315-2325. doi:10.1242/dev.125.12.2315

Hall, M. L., Givens, S., Santosh, N., Iacovino, M., Kyba, M. and Ogle, B. M. (2022). Laminin 411 mediates endothelial specification via multiple signaling axes that converge on β-catenin. *Stem Cell Rep.* **17**, 569-583. doi:10.1016/j.stemcr.2022.01.005

Horejs, C.-M., Serio, A., Purvis, A., Gormley, A. J., Bertazzo, S., Poliniewicz, A., Wang, A. J., DiMaggio, P., Hohenester, E. and Stevens, M. M. (2014). Biologically-active laminin-111 fragment that modulates the epithelial-to-mesenchymal transition in embryonic stem cells. *Proc. Natl. Acad. Sci. USA* **111**, 5908-5913. doi:10.1073/pnas.1403139111

Hyysalo, A., Ristola, M., Mäkinen, M. E.-L., Häyrynen, S., Nykter, M. and Narkilahti, S. (2017). Laminin α5 substrates promote survival, network formation and functional development of human pluripotent stem cell-derived neurons in vitro. *Stem Cell Res.* **24**, 118-127. doi:10.1016/j.scr.2017.09.002

Imayoshi, I., Sakamoto, M., Yamaguchi, M., Mori, K. and Kageyama, R. (2010). Essential roles of Notch signaling in maintenance of neural stem cells in developing and adult brains. *J. Neurosci.* **30**, 3489-3498. doi:10.1523/JNEUROSCI.4987-09.2010

Inta, D., Cameron, H. A. and Gass, P. (2015). New neurons in the adult striatum: from rodents to humans. *Trends Neurosci.* **38**, 517-523. doi:10.1016/j.tins.2015.07.005

Iwano, T., Masuda, A., Kiyonari, H., Enomoto, H. and Matsuzaki, F. (2012). Prox1 postmitotically defines dentate gyrus cells by specifying granule cell identity over CA3 pyramidal cell fate in the hippocampus. *Development* **139**, 3051-3062.

Kiritsi, D., Has, C. and Bruckner-Tuderman, L. (2013). Laminin 332 in junctional epidermolysis bullosa. *Cell Adh. Migr.* **7**, 135-141. doi:10.4161/cam.22418

Knoth, R., Singec, I., Ditter, M., Pantazis, G., Capetian, P., Meyer, R. P., Horvat, V., Volk, B. and Kempermann, G. (2010). Murine Features of Neurogenesis in the Human Hippocampus across the Lifespan from 0 to 100 Years. *PLoS One* **5**, e8809. doi:10.1371/journal.pone.0008809

Lavado, A., Lagutin, O. V., Chow, L. M. L., Baker, S. J. and Oliver, G. (2010). Prox1 is required for granule cell maturation and intermediate progenitor maintenance during brain neurogenesis. *PLoS Biol.* **8**, e1000460. doi:10.1371/journal.pbio.1000460

Lee, S. M., Tole, S., Grove, E. and McMahon, A. P. (2000). A local Wnt-3a signal is required for development of the mammalian hippocampus. *Development* **127**, 457-467. doi:10.1242/dev.127.3.457

Lester, A. W., Moffat, S. D., Wiener, J. M., Barnes, C. A. and Wolbers, T. (2017). The aging navigational system. *Neuron* **95**, 1019-1035. doi:10.1016/j.neuron.2017.06.037

Long, K. R. and Huttner, W. B. (2019). How the extracellular matrix shapes neural development. *Open Biol.* **9**, 180216. doi:10.1098/rsob.180216

Long, K., Moss, L., Laursen, L., Boulter, L. and Ffrench-Constant, C. (2016). Integrin signalling regulates the expansion of neuroepithelial progenitors and neurogenesis via Wnt7a and Decorin. *Nat. Commun.* **7**, 10354. doi:10.1038/ncomms10354

Lugert, S., Basak, O., Knuckles, P., Haussler, U., Fabel, K., Götz, M., Haas, C. A., Kempermann, G., Taylor, V. and Giachino, C. (2010). Quiescent and active hippocampal neural stem cells with distinct morphologies respond selectively to physiological and pathological stimuli and aging. *Cell Stem Cell* **6**, 445-456. doi:10.1016/j.stem.2010.03.017

Ma, W., Tavakoli, T., Derby, E., Serebryakova, Y., Rao, M. S. and Mattson, M. P. (2008). Cell-extracellular matrix interactions regulate neural differentiation of human embryonic stem cells. *BMC Dev. Biol.* **8**, 90. doi:10.1186/1471-213X-8-90

Machon, O., Backman, M., Machonova, O., Kozmik, Z., Vacik, T., Andersen, L. and Krauss, S. (2007). A dynamic gradient of Wnt signaling controls initiation of neurogenesis in the mammalian cortex and cellular specification in the hippocampus. *Dev. Biol.* **311**, 223-237. doi:10.1016/j.ydbio.2007.08.038

Martins, M., Galfrè, S., Terrigno, M., Pandolfini, L., Appolloni, I., Dunville, K., Marranci, A., Rizzo, M., Mercatanti, A., Poliseno, L. et al. (2021). A eutherian-specific microRNA controls the translation of Satb2 in a model of cortical differentiation. *Stem Cell Rep.* **16**, 1496-1509. doi:10.1016/j.stemcr.2021.04.020

Ming, G. and Song, H. (2011). Adult neurogenesis in the mammalian brain: significant answers and significant questions. *Neuron* **70**, 687-702. doi:10.1016/j.neuron.2011.05.001

Mitchelmore, C., Kjaerulff, K. M., Pedersen, H. C., Nielsen, J. V., Rasmussen, T. E., Fisker, M. F., Finsen, B., Pedersen, K. M. and Jensen, N. A. (2002). Characterization of two novel nuclear BTB/POZ domain zinc finger isoforms. Association with differentiation of hippocampal neurons, cerebellar granule cells, and macroglia. *J. Biol. Chem.* **277**, 7598-7609. doi:10.1074/jbc.M110023200

Nakashima, Y. and Omasa, T. (2016). What kind of signaling maintains Pluripotency and viability in human-induced pluripotent stem cells cultured on Laminin-511 with serum-free medium? *BioResearch Open Access* **5**, 84-93. doi:10.1089/biores.2016.0001

Nascimento, M. A., Sorokin, L. and Coelho-Sampaio, T. (2018). Fractone bulbs derive from ependymal cells and their laminin composition influence the stem cell niche in the subventricular zone. *J. Neurosci.* **38**, 3880-3889. doi:10.1523/JNEUROSCI.3064-17.2018

Naujok, O., Lentes, J., Diekmann, U., Davenport, C. and Lenzen, S. (2014). Cytotoxicity and activation of the Wnt/beta-catenin pathway in mouse embryonic stem cells treated with four GSK3 inhibitors. *BMC Res. Notes* **7**, 273. doi:10.1186/1756-0500-7-273

Ni, Y., Liu, B., Wu, X., Liu, J., Ba, R. and Zhao, C. (2021). FOXG1 directly suppresses Wnt5a during the development of the hippocampus. *Neurosci. Bull.* **37**, 298-310. doi:10.1007/s12264-020-00618-z

Nielsen, J. V., Thomassen, M., Møllgård, K., Noraberg, J. and Jensen, N. A. (2014). Zbtb20 defines a hippocampal neuronal identity through direct repression of genes that control projection neuron development in the isocortex. *Cereb. Cortex* **24**, 1216-1229. doi:10.1093/cercor/bhs400

Nirwane, A. and Yao, Y. (2019). Laminins and their receptors in the CNS: Laminins and their receptors in the CNS. *Biol. Rev.* **94**, 283-306. doi:10.1111/brv.12454

Noguchi, H., Castillo, J. G., Nakashima, K. and Pleasure, S. J. (2019). Suppressor of fused controls perinatal expansion and quiescence of future dentate adult neural stem cells. *Elife* **8**, e42918. doi:10.7554/eLife.42918

Palmer, T. D., Willhoite, A. R. and Gage, F. H. (2000). Vascular niche for adult hippocampal neurogenesis. *J. Comp. Neurol.* **425**, 479-494. doi:10.1002/1096-9861(20001002)425:4<479::AID-CNE2>3.0.CO;2-3

Patro, R., Duggal, G., Love, M. I., Irizarry, R. A. and Kingsford, C. (2017). Salmon provides fast and bias-aware quantification of transcript expression. *Nat. Methods* **14**, 417-419. doi:10.1038/nmeth.4197

Pencea, V., Bingaman, K. D., Freedman, L. J. and Luskin, M. B. (2001). Neurogenesis in the subventricular zone and rostral migratory stream of the neonatal and adult primate forebrain. *Exp. Neurol.* **172**, 1-16. doi:10.1006/exnr.2001.7768

Quattrocolo, G., Fishell, G. and Petros, T. J. (2017). Heterotopic transplantations reveal environmental influences on interneuron diversity and maturation. *Cell Rep.* **21**, 721-731. doi:10.1016/j.celrep.2017.09.075

Rosenthal, E. H., Tonchev, A. B., Stoykova, A. and Chowdhury, K. (2012). Regulation of archicortical arealization by the transcription factor Zbtb20. *Hippocampus* **22**, 2144-2156. doi:10.1002/hipo.22035

Sakaguchi, H., Kadoshima, T., Soen, M., Narii, N., Ishida, Y., Ohgushi, M., Takahashi, J., Eiraku, M. and Sasai, Y. (2015). Generation of functional hippocampal neurons from self-organizing human embryonic stem cell-derived dorsomedial telencephalic tissue. *Nat. Commun.* **6**, 8896. doi:10.1038/ncomms9896

Sarkar, A., Mei, A., Paquola, A. C. M., Stern, S., Bardy, C., Klug, J. R., Kim, S., Neshat, N., Kim, H. J., Ku, M. et al. (2018). Efficient generation of CA3 neurons from human pluripotent stem cells enables modeling of hippocampal connectivity in vitro. *Cell Stem Cell* **22**, 684-697.e9. doi:10.1016/j.stem.2018.04.009

Sasaki, T., Takagi, J., Giudici, C., Yamada, Y., Arikawa-Hirasawa, E., Deutzmann, R., Timpl, R., Sonnenberg, A., Bächinger, H. P. and Tonge, D. (2010). Laminin-121—recombinant expression and interactions with integrins. *Matrix Biol.* **29**, 484-493. doi:10.1016/j.matbio.2010.05.004

Shi, Y., Kirwan, P., Smith, J., Robinson, H. P. C. and Livesey, F. J. (2012a). Human cerebral cortex development from pluripotent stem cells to functional excitatory synapses. *Nat. Neurosci.* **15**, 477-486. doi:10.1038/nn.3041

Shi, Y., Kirwan, P. and Livesey, F. J. (2012b). Directed differentiation of human pluripotent stem cells to cerebral cortex neurons and neural networks. *Nat. Protoc.* **7**, 1836-1846. doi:10.1038/nprot.2012.116

Simon, R., Brylka, H., Schwegler, H., Venkataramanappa, S., Andratschke, J., Wiegreffe, C., Liu, P., Fuchs, E., Jenkins, N. A., Copeland, N. G. et al. (2012). A dual function of Bcl11b/Ctip2 in hippocampal neurogenesis. *EMBO J.* **31**, 2922-2936. doi:10.1038/emboj.2012.142

Song, J., Sun, J., Moss, J., Wen, Z., Sun, G. J., Hsu, D., Zhong, C., Davoudi, H., Christian, K. M., Toni, N. et al. (2013). Parvalbumin interneurons mediate neuronal circuitry–neurogenesis coupling in the adult hippocampus. *Nat. Neurosci.* **16**, 1728-1730. doi:10.1038/nn.3572

Terrigno, M., Busti, I., Alia, C., Pietrasanta, M., Arisi, I., D'Onofrio, M., Caleo, M. and Cremisi, F. (2018). Neurons generated by mouse ESCs with hippocampal or cortical identity display distinct projection patterns when co-transplanted in the adult brain. *Stem Cell Rep.* **10**, 1016-1029. doi:10.1016/j.stemcr.2018.01.010

Urbán, N. and Guillemot, F. (2014). Neurogenesis in the embryonic and adult brain: same regulators, different roles. *Front. Cell. Neurosci.* **8**, 396. doi:10.3389/fncel.2014.00396

van Praag, H., Shubert, T., Zhao, C. and Gage, F. H. (2005). Exercise enhances learning and hippocampal neurogenesis in aged mice. *J. Neurosci.* **25**, 8680-8685. doi:10.1523/JNEUROSCI.1731-05.2005

Xie, Z., Ma, X., Ji, W., Zhou, G., Lu, Y., Xiang, Z., Wang, Y. X., Zhang, L., Hu, Y., Ding, Y.-Q. et al. (2010). Zbtb20 is essential for the specification of CA1 field identity in the developing hippocampus. *Proc. Natl. Acad. Sci. USA* **107**, 6510-6515. doi:10.1073/pnas.0912315107

Yu, D. X., Di Giorgio, F. P., Yao, J., Marchetto, M. C., Brennand, K., Wright, R., Mei, A., McHenry, L., Lisuk, D., Grasmick, J. M. et al. (2014a). Modeling hippocampal neurogenesis using human pluripotent stem cells. *Stem Cell Rep.* **2**, 295-310. doi:10.1016/j.stemcr.2014.01.009

Yu, D. X., Marchetto, M. C. and Gage, F. H. (2014b). How to make a hippocampal dentate gyrus granule neuron. *Development* **141**, 2366-2375. doi:10.1242/dev.096776